Bull. Inst. Chem. Res., Kyoto Univ., Vol. 59, No. 3, 1981

Mechanical Properties of PbO-B_2O_3 Immiscible Glasses

Noboru MIYATA and Hiroshi JINNO*

Received March 31, 1981

The present study is concerned with the mechanical properties of phase-separated glasses with particulate microstructure. Vickers hardness, flexural strength, fracture toughness and fracture surface energy of PbO–B_2O_3 immiscible glasses were measured. The experimental results were interpreted in terms of the properties and amounts of the constituent phases and the microstructural effects.

KEY WORDS: Phase-separated glasses/ Glass matrix, particulate composites/ Vickers hardness/ Strength/ Fracture toughness/ Fracture surface energy/

I. INTRODUCTION

In the last decade, a number of basic studies have been made to relate mechanical properties of brittle matrix, particulate composites to both the microstructural parameters and the properties and amounts of the constituent phases. These studies have shown that the mechanical properties of such materials can be influenced not only by the amount, size and shape of the dispersed particles but also the relative mechanical and physical properties of the particle and matrix[1,2] However, it is still difficult to generalize the effect of a second-phase dispersion on the deformation and fracture behaviour of brittle materials.

It is the purpose of the present investigation, by concentrating upon one simple two-phase glass system, to gain further understanding of the basic deformation and fracture mechanisms of brittle matrix, particulate composites. The immiscible glass compositions in the PbO-B_2O_3 system was chosen for study. This system has one of the best characterized immiscible phase boundaries, which lies between about 1–44 wt% PbO.[3~5]

II. EXPERIMENTAL PROCEDURE

The glass samples containing 0 to 45 wt% PbO were prepared. Sample fabrication and microstructural characterization technique were already described elsewhere.[6,7]

1. Hardness

Finely polished specimens about 3 mm thick were used for indentation hardness measurements. Indentation tests were performed using a Vickers diamond pyramid

* 宮田 昇, 神野 博: Department of Industrial Chemistry, Faculty of Engineering, Kyoto University, Sakyo-ku, Kyoto.

with a micro-hardness tester at room temperature under a dry N_2 environment. Twenty indentations were made for each specimen with a time of 5 s at full load of a 100 g weight.

2. Strength

Flexural strength was measured using rectangular bars 8 by 4 by 40 mm. Measurements were made with a testing machine using three-point loading over a 32 mm span. All measurements were made in air at room temperature at a loading rate of 0.5 mm/min. Six to ten specimens were fractured for each PbO content.

3. Fracture Toughness and Fracture Surface Energy

Fracture toughness values were determined using the three-point bend test of a single-edge-notched-beam(SENB) along with the Vickers indentation technique. The latter method has been developed over the last several years based upon a fracture mechanics analysis of the indentation fracture problem.[8~10] The applicability of the indentation technique to fracture toughness evaluation of the present phase-separated glasses has been recently examined by the authors.[6] The purpose of additional use of the indentation method is to obtain toughness values at lower PbO composition range in which SENB specimen fabrication is rather laborious and difficult.

SENB specimens 8 by 4 by 40 mm were prepared. Specimens were tested in three-point bending over a 32 mm span at a cross-head speed of 0.5 mm/min. All measurements were carried out in air at room temperature. At least 6 specimens for each PbO content were tested. Fracture toughness values K_{IC} were evaluated from specimen dimensions and fracture load using the equation given by Brown and Srawley.[11]

The fracture toughness determinations by indentation testing were made on finely polished specimens similar to those used for hardness measurements. Indentation tests were performed using a Vickers diamond pyramid with a micro-hardness tester at room temperature under a dry N_2 environment. The surface traces of the cracks extending from the impression corners were measured by optical microscopy about 30 minutes after the load was removed. At least 30 separate indentation fracture patterns were produced on each specimen surface under an indenter load of 1 kg. Relative toughness values $k\,K_{IC}$ (k: correction factor) were evaluated from indenter load and produced crack dimension using the equation given by Lawn and Fuller.[8] The correction factor k was estimated by fitting the indentation data to toughness values obtained from the three-point bend test. Using the value for k thus estimated, absolute values for fracture toughness were evaluated for glass samples to which the three-point bending technique was not applied.

Assuming that conditions of plane strain are met, the fracture surface energy Γ is given by;[12]

$$\Gamma = \frac{(1-\nu^2)K_{IC}^2}{2E} \tag{1}$$

where E is the Young's modulus and ν is the Poisson's ratio. The elastic properties of

the present glasses in relation to their microstructures have been studied in detail by Shaw and Uhlmann.[13] Using their published data for Young's modulus and Poisson's ratio, the fracture toughness K_{IC} was converted to fracture surface energy according to Eq. (1).

III. EXPERIMENTAL RESULTS

1. Microstructure

In Table I are summarized the results of the structural characterization by electron microscopy. As shown by Shaw and Uhlmann,[4] present glasses are typical particulate composites which are composed of the two end-member phases. For the B_2O_3-rich region (about 1–20 wt% PbO) within the miscibility gap, B_2O_3-rich phase forms continuous phase, while for the PbO-rich region (about 30–44 wt% PbO), PbO-rich phase is continuous. In both regions, the volume fractions of the PbO-rich phase evaluated from electron micrographs agreed quite well with those calculated theoretically from densities and compositions.[7]

Table I. Microstructural characteristics of PbO–B_2O_3 immiscible glasses

wt% PbO	Volume fraction of PbO-rich phase	Vol. frac. of dispersed particles ϕ	Dispersed particle size $D/\mu m$	Microstructure
0	—	—	—	
5	0.05	0.05		
10	0.13	0.13	0.17	PbO-rich spherical particles
13	0.18	0.18	0.18	in a B_2O_3-rich matrix
17	0.25	0.25	0.20	
	—	—	—	
32	0.59	0.41	0.53	
36	0.71	0.29	0.35	
40	0.84	0.16	0.40	B_2O_3-rich spherical particles
41	0.88	0.12		in a PbO-rich matrix
45	—	—	—	

2. Mechanical Properties

The results of mechanical property measurements are listed in Table II. The values for Young's modulus were obtained by interpolation of the experimental modulus data over the miscibility gap, published by Shaw and Uhlmann.[13] As for glass compositions less than 5 wt% PbO, strength measurements were not carried out because rectangular bar specimens could not be fabricated in a controlled manner.

The size of the critical crack from which catastrophic failure initiates can be calculated with knowledge of the strength and fracture toughness. By arranging Griffith's fracture equation, the critical crack size can be expressed as;[14]

Table II. Mechanical property data for $PbO-B_2O_3$ immiscible glasses

wt% PbO	Vickers hardness H/GPa	Fracture toughness K_{IC}/MNm$^{-3/2}$	Young's modulus[a] E/GPa	Fracture surface energy Γ/Jm^{-2}	Flexural strength S/MPa	Calculated critical crack size a/μm
0	1.21	0.954	17.3	24.5		
5	1.28	0.926	18.7	21.4	104	50
10	1.43	0.856	20.2	16.9	101	45
13	1.45	0.828	21.0	15.2	106	38
17	1.55	0.833	22.3	14.5	98.3	45
32	2.35	1.59	31.2	37.6	89.4	198
35			34.5		104	
36	2.76	1.38	36.2	24.4	102	114
40	2.82	1.33	44.5	18.4	86.3	149
41	3.15		47.2			
45	3.63	0.906	60.4	6.30	72.6	98

a) Data from Shaw and Uhlmann[13]

$$a=\frac{Y^2K_{IC}^2}{2S^2} \tag{2}$$

where a is the crack depth in the surface, S is the fracture stress and Y is a constant which depends upon the crack and specimen geometry ($Y=1.12$ for a surface half-penny crack[14]). Assuming that failure is initiated from a penny-shaped surface crack, the critical crack sizes were calculated from Eq. (2). The results are shown in the last column of Table II.

IV. DISCUSSION

1. Properties of the End-member Phase

In Table III are shown some mechanical properties for the end-member phases, estimated by interpolation of the experimental data listed in Table II. Table III also includes thermal expansion coefficient data compiled by Takamori.[15]

2. Hardness Behaviour

Indentation hardness is defined as the load divided by the pyramidal area of indentation, the mean pressure under the indenter. That is, the hardness quantifies the resistance to deformation of materials and can be considered as convenient material parameter for characterizing deformation process. Recently, Miyata and Jinno[16] tried to analyze the indentation hardness of glass matrix, particulate composites regarding glasses as elastic-plastic materials on a microscopic scale. Based upon Marsh's theory[17] of indentation, expressions were formulated for indentation hardness of glass matrix composites containing spherical crystalline or glass particles. When hard particles are dispersed in a soft glass matrix, it is assumed that the deformation

Table III. Estimated mechanical data for the end-member phases

		End-member phases	
		1 wt% PbO glass	44 wt% PbO glass
Young's modulus[a)]	E/GPa	17.5	56.5
Poisson's ratio[a)]	ν	0.26	0.27
Fracture toughness	K_{IC}/MNm$^{-3/2}$	0.947	0.960
Fracture surface energy	Γ/Jm^{-2}	23.9	7.56
Vickers hardness	H/GPa	1.23	3.53
Flow stress[b)]	σ_y/GPa	0.716	1.92
Thermal expansion coefficient[c)]	α/10^{-6}°C^{-1}	~14	~ 7

a) After Shaw and Uhlmann[13)]
b) Evaluated from Marsh's theory[17)]
c) After Takamori[15)]

of second-phase particles can not be accomodated to the plastic flow in the matrix. The hardness of the composite H can be expressed, for a dilute concentration of dispersed phase, as;

$$\frac{H}{H_m}=\left(1+\frac{Q-1}{1-Q\phi}\phi\right)\left(1+\kappa\ln\frac{1-Q\phi}{(1-\alpha\phi)(1-\phi)}\right) \tag{3}$$

with

$$\kappa=B\sigma_{ym}/H_m$$

$$Q=\frac{15(1-\nu_m)\mu_p}{(7-5\nu_m)\mu_m+(8-10\nu_m)\mu_p}$$

$$\alpha=\frac{15(1-\nu_m)}{7-5\nu_m}(Q-1)$$

where H_m is the hardness of the matrix without a dispersion, μ is the shear modulus, σ_{ym} is the flow stress of the matrix, and B is a constant equal to 0.60; subscripts m and p refer to the matrix and particle, respectively. The constant κ which depends upon the flow stress and hardness of a glass matrix can be estimated at 0.3 to 0.4 for most glasses.[16)] When soft particles are dispersed in a hard glass matrix, on the other hand, it can be assumed that the dispersed particles do not act as obstacles to the deformation after the onset of the plastic flow in the matrix. For this case, the theory predicts that the hardness and elastic moduli vary in parallel with volume fraction of dispersed particles. The hardness is given by;

$$\frac{H}{H_m}=1+\frac{\phi}{\dfrac{\mu_m}{\mu_p-\mu_m}+\dfrac{6(K_m+2\mu_m)(1-\phi)}{5(3K_m+4\mu_m)}} \tag{4}$$

where K is the bulk modulus.

For glass compositions on the B_2O_3-rich side within the miscibility gap, the dispersed second-phase has higher elastic moduli and higher flow stress. In addition, the glasses in this composition range present relatively small volume fractions of

dispersed phase. It is then expected that the hardness behaviour follows Eq. (3) derived for a composite consisting of hard particles/soft glass matrix. On the other hand, for glass compositions on the PbO-rich side within the miscibility gap, it is expected that the presence of the second-phase dispersion causes a reduction of the hardness and its behaviour is explained following Eq. (4). In Fig. 1, the experimental hardness data for the glasses in both composition ranges are plotted against the volume fraction of dispersed particles. It is seen from Fig. 1 that the experimental data are in fair agreement with the theoretical predictions in both regions.

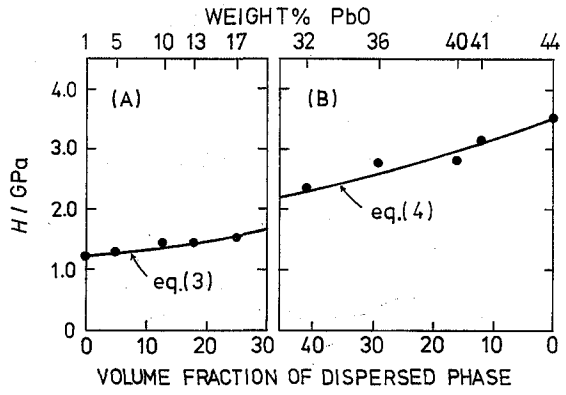

Fig. 1. Variation of Vickers hardness with volume fraction of dispersed phase for (A) glasses consisting of PbO-rich particles/B_2O_3-rich matrix and (B) glasses consisting of B_2O_3-rich particles/PbO-rich matrix.

3. Fracture Behaviour

It has been suggested that second-phase dispersions in a brittle material can increase fracture surface energy and fracture strength. The increase in fracture surface energy in some brittle particulate composites has been related to the change in crack shape caused by impedance of the crack front by the second-phase obstacles. Lange[18] proposed, based upon a 'line tension concept', a mechanism of the momentary pinning of the moving crack front by obstacles, and provided an expression for the fracture surface energy of a brittle particulate composite. Evans[19] elaborated this theory and calculated the line tension contribution to the fracture surface energy as a function of the ratios of the obstacle dimensions and the obstacle spacing, where the obstacles can be considered 'impenetrable'. He concluded that line tension may be the major contribution to the increase in fracture surface energy of brittle matrix/brittle particle composites.

However, second-phase dispersions must have a variety of microstructural effects and they can also lower fracture surface energy and strength.[2] Second-phase particles (or pores) can act as stress concentrators in particulate composites when elastic moduli and thermal expansion coefficient of particles are different from those of the matrix.[20,21] It is then possible that localized stress fields around and within the particles determine the fracture path and aid, in certain circumstances, crack pro-

pagation which results in a lowering of the fracture surface energy. Here, we will interpret the data for fracture surface energy and strength, taking into account possible fracture paths in glasses under study.

3.1. Fracture path

In the presence of localized stress fields around and within particles due to elastic and thermal expansion mismatch between particle and matrix, the propagating primary crack can either go through or circumvent the particles depending upon the differential thermal expansion, differential elastic properties and differential fracture surface energy of the phases.[7] The fracture paths in the present two-phase glasses can be deduced on the basis of the discussions given in Ref. 7 and are shown schematically in Fig. 2.

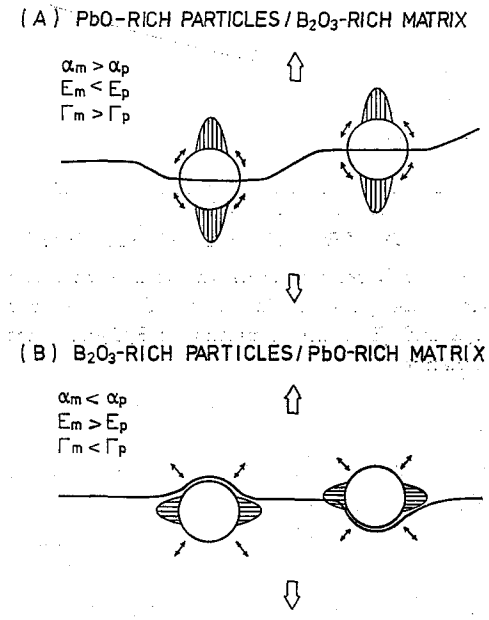

Fig. 2. Schematic of fracture paths expected for PbO–B_2O_3 immiscible glasses.[7] Arrows around each particle represent residual thermal stresses in the matrix. Shaded areas represent stress-concentrated regions in the matrix produced by elastic mismatch. The subscripts m and p refer to the matrix and particle, respectively.

3.2. Glasses consisting of PbO-rich particles/B_2O_3-rich matrix

For glass compositions on the B_2O_3-rich side within the miscibility gap, the fracture path is expected to go through the particles. Therefore, the Lange-Evans theory is inapplicable to the present case.

Let us now consider the contribution of second-phase particles to the fracture surface energy when the particles are considered 'penetrable'. If we assume that the crack will simply pass through the average areas of each phase, stereological considerations lead to the following expression for the fracture surface energy of composites;

$$\Gamma = \Gamma_m - (\Gamma_m - \Gamma_p)\phi. \quad (5)$$

However, it is unlikely that the crack passes through the stereological average areas of the two phases. It can be assumed that the crack will seek the path having minimum area of the matrix with higher fracture surface energy than the particles. That is, the crack will suffer local deviation from its main plane, seeking preferentially the nearest-neighbour distances between particles. If this crack propagation mechanism occurs, the volume fraction of dispersed phase in Eq. (5) should be replaced by a local volume fraction of dispersed particles ϕ_l which we define as;

$$\phi_l = (\bar{L}_3/\Delta_3)^3 \quad (6)$$

where $\bar{L}_3$ is the mean intercept length of randomly distributed particles and Δ_3 is the average distance between nearest-neighbour pairs of particles in a volume. For a dilute dispersion of randomly distributed spherical particles of diameter D, the nearest-neighbour distance in a volume is approximated as $\Delta_3 \simeq 0.554\ (\pi D^2\lambda/4)^{1/3}$ where λ is the mean free distance between particles.[22] The quantity λ is expressed as $2D(1-\phi)/(3\phi)$ for randomly distributed spherical particles[23] and can be approximated as $2D/(3\phi)$ for small volume fractions of dispersed particles. Then Δ_3 can be written as $\Delta_3 \simeq 0.447\mathrm{D}/\phi^{1/3}$. On the other hand, $\bar{L}_3$ is given by $2D/3$ for randomly dispersed spheres.[23] Hence it follows from Eq. (6);

$$\phi_l = (\bar{L}_3/\Delta_3)^3 = 3.33\phi \quad (7)$$

and fracture surface energy is given by;

$$\begin{aligned}\Gamma &= \Gamma_m - (\Gamma_m - \Gamma_p)\phi_l \\ &= \Gamma_m - 3.33(\Gamma_m - \Gamma_p)\phi.\end{aligned} \quad (8)$$

In Fig. 3, the reduced fracture surface energies obtained for the glasses under consideration are plotted against the volume fraction of dispersed particles. Theoretical prediction from Eq. (8) is represented by a solid line, established by taking the values as $\Gamma_m = 23.9\ \mathrm{Jm^{-2}}$ and $\Gamma_p = 7.56\ \mathrm{Jm^{-2}}$. For comparison purpose, Eq. (5) is also represented in the figure by a broken line. As expected, the experimental data agree quite well with the theoretical prediction over the volume fraction range lower than 0.15. The observed deviations in the volume fraction range higher than 0.15 can be attributed to the fact that Eq. (8) is no more valid for larger volume fractions of dispersed particles.

Table II suggests that the present dispersed fine particles being considered 'penetrable' have no effect on the critical crack size, although they can influence the fracture surface energies. Thus, the strength and fracture toughness in the present type of composites vary in parallel with volume fraction of dispersed particles under the same testing condition.

3.3 Glasses consisting of B_2O_3-rich particles/PbO-rich matrix

As shown in Fig. 2(B), the fracture path in these two-phase composites is considered to circumvent the particles. It is then expected that observed increase in

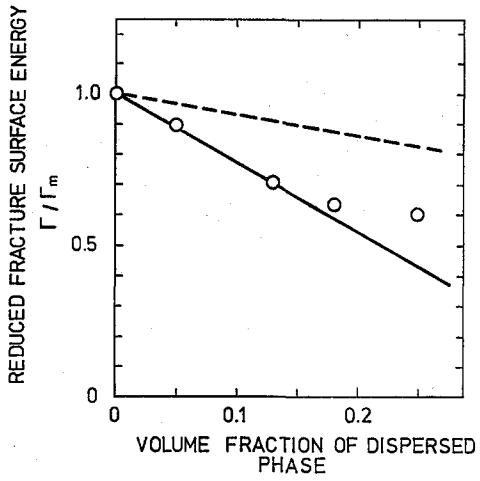

Fig. 3. Reduced fracture surface energy for glasses consisting of PbO-rich particles/B_2O_3-rich matrix plotted against the volume fraction of dispersed particles. Solid line represents Eq. (8) and broken line, Eq. (5).

fracture surface energy with increasing second-phase particles can be explained by the application of the Lange-Evans theory.[18,19]

Lange[18] found that the fracture surface energy is linearly related to the reciprocal of the mean free path between particles;

$$\Gamma = \Gamma_m + \tau/\lambda \tag{9}$$

where τ is the line tension of the crack front. Evans[19] elaborated Lange's theory and calculated the line tension contribution to the fracture surface energy assuming 'impenetrable' particles. In Fig. 4, the fracture surface energies for glasses consisting of B_2O_3-rich particles/PbO-rich matrix are plotted against the ratio of the particle size to the particle spacing, D/λ. Theoretical line tension contribution calculated from Evans' theory is drawn in the figure by a solid curve. It is found that the measured fracture surface energy varies with D/λ in a similar manner to the predicted line tension contribution. This indicates that the particles act as 'impenetrable' obstacles and the line tension may be the major contribution to the increase in the fracture surface energy with second-phase particles.

The critical crack size calculated for the present glasses should be regarded as invariant with volume fraction of dispersed B_2O_3-rich particles. The dispersed particle size is found to be much smaller than the crack size in the homogeneous glass, and the impenetrable second-phase dispersion appears to have no effect on the crack size. This suggests that the crack size in particulate composites is invariant with their microstructure regardless of the 'particle impenetrability', when the critical crack size in the host glass without a dispersed phase is much larger than the particle size. It is then concluded that the critical crack size in the present glasses remains constant as long as the testing condition is identical, and observed increases in strength result entirely from increases in fracture toughness.

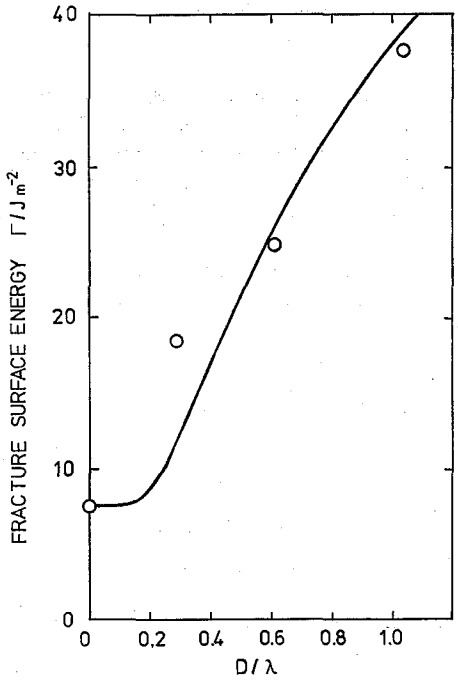

Fig. 4. Fracture surface energy for glasses consisting of B_2O_3-rich particles/PbO-rich matrix as a function of the ratio of the particle size to the particle spacing, D/λ. Solid curve represents the line tension contribution calculated from Evans' theory.[19]

V. CONCLUSION

Vickers hardness, flexural strength, fracture toughness and fracture surface energy were measured for lead borate glasses having compositions within the miscibility gap in the PbO-B_2O_3 system. The microstructure consists of PbO-rich particles/B_2O_3-rich matrix for glass compositions on the B_2O_3rich side of the miscibility gap, and conversely B_2O_3-rich particles/PbO-rich matrix for glass compositions on the PbO-rich side of the gap. The deformation and fracture behaviour observed in the present two types of particulate composites could be best interpreted in terms of the properties and amounts of each phase and the microstructural effects.

REFERENCES

(1) F. F. Lange, "Composite Materials", Vol. 5, L. J. Broutman Ed., Academic Press, New York, 1974, p. 1.
(2) R. W. Rice, "Treatise on Materials Science and Technology", Vol. 11, R. K. MacCrone Ed., Academic Press, New York, 1977, p. 199.
(3) J. Zarzycki and F. Naudin, *Phys. Chem. Glasses*, **8**, 11 (1967).
(4) R. R. Shaw and D. R. Uhlmann, *J. Non-Cryst. Sotids*, **1**, 474 (1969).
(5) R. R. Shaw and J. F. Breedis, *J. Am. Ceram. Soc.*, **55**, 422 (1972).

(6) N. Miyata and H. Jinno, *J. Non-Cryst. Solids*, **38/39**, 391 (1980).
(7) N. Miyata and H. Jinno, *J. Mater. Sci.*, in press.
(8) B. R. Lawn and E. R. Fuller, *ibid.*, **10**, 2016 (1975).
(9) A. G. Evans and E. A. Charles, *J. Am. Ceram. Soc.*, **59**, 371 (1976).
(10) M. V. Swain, J. T. Hagan, and J. E. Field, *J. Mater. Sci.*, **12**, 1914 (1977).
(11) W. F. Brown, Jr. and J. E. Srawley, "Plane Strain Crack Toughness Testing of High Strength Metallic Materials", ASTM STP 410, ASTM, Philadelphia, 1966.
(12) A. S. Tetelman and A. J. McEvily, Jr., "Fracture of Structural Materials", John Wiley and Sons, New York, 1967.
(13) R. R. Shaw and D. R. Uhlmann, *J. Non-Cryst. Solids*, **5**, 237 (1971).
(14) J. J. Mecholsky, S. W. Freiman, and R. W. Rice, *J. Mater. Sci.*, **11**, 1310 (1976).
(15) T. Takamori, "Treatise on Materials Science and Technology", Vol. 17, M. Tomozawa *et al.* Ed., Academic Press, New York, 1979, p. 173.
(16) N. Miyata and H. Jinno, *J. Mater. Sci.*, in press.
(17) D. M. Marsh, *Proc. Roy. Soc.* (*London*), **A279**, 420 (1964).
(18) F. F. Lange, *Phil. Mag.*, **22**, 983 (1970).
(19) A. G. Evans, *ibid.*, **26**, 1327 (1972).
(20) J. Selsing, *J. Am. Ceram. Soc.*, **44**, 419 (1961).
(21) J. N. Goodier, *J. Appl. Mech.*, **1**, 39 (1933).
(22) E. E. Underwood, "Quantitative Stereology", Addison-Wesley, Reading, Mass., 1970, p. 80.
(23) R. L. Fullman, *Trans. AIME*, **197**, 447 (1953).